Science Bulletin 67 (2022) 748–754

Contents lists available at ScienceDirect

Science Bulletin

journal homepage: www.elsevier.com/locate/scib

Science Bulletin
www.scibull.com

Article

Mid-mantle water transportation implied by the electrical and seismic properties of ε-FeOOH

Yukai Zhuang [a,b,1], Bo Gan [b,1], Zhongxun Cui [a], Ruilian Tang [a,c], Renbiao Tao [a], Mingqiang Hou [d], Gang Jiang [b], Catalin Popescu [e], Gaston Garbarino [f], Youjun Zhang [b,g,*], Qingyang Hu [a,h,*]

[a] Center for High Pressure Science and Technology Advanced Research, Beijing 100094, China
[b] Institute of Atomic and Molecular Physics, Sichuan University, Chengdu 610065, China
[c] School of Materials Science and Engineering, Changchun University of Science and Technology, Changchun 130022, China
[d] State Key Laboratory of Geodesy and Earth's Dynamics, Innovation Academy for Precision Measurement Science and Technology, Chinese Academy of Sciences, Wuhan 430077, China
[e] Consorcio para la Construcción, Equipamiento y Explotación del Laboratorio de Luz de Sincrotrón, Cerdanyola del Vallès, Barcelona 08290, Spain
[f] European Synchrotron Radiation Facility, Grenoble 38000, France
[g] International Center for Planetary Science, College of Earth Sciences, Chengdu University of Technology, Chengdu 610059, China
[h] Center for Excellence in Deep Earth Science, Guangzhou Institute of Geochemistry, Chinese Academy of Sciences, Guangzhou 510640, China

ARTICLE INFO

Article history:
Received 10 August 2021
Received in revised form 19 November 2021
Accepted 22 November 2021
Available online 4 December 2021

Keywords:
Mid-lower mantle
Electrical conductivity
Seismic velocity
Heterogeneity

ABSTRACT

Water in the mantle transition zone and the core-mantle boundary plays a key role in Earth's stratification, volatile cycling, and core formation. If water transportation is actively running between the aforementioned layers, the lower mantle should contain water channels with distinctive seismic and/or electromagnetic signatures. Here, we investigated the electrical conductivity and sound velocity of ε-FeOOH up to 71 GPa and 1800 K and compared them with global tomography data. An abrupt three-order jump of electrical conductivity was observed above 50 GPa, reaching 1.24(12) × 10^3 S/m at 61 GPa. Meanwhile, the longitudinal sound velocity dropped by 16.8% in response to the high-to-low spin transition of Fe^{3+}. The high-conductivity and low-sound velocity of ε-FeOOH match the features of heterogenous scatterers in the mid-lower mantle. Such unique properties of hydrous ε-FeOOH, or possibly other Fe-enriched phases can be detected as evidence of active water transportation in the mid-lower mantle.

1. Introduction

A substantial ocean mass of water may reside in Earth's deep interiors [1,2]. For example, the mantle transition zone is the home to water-bearing wadsleyite and ringwoodite, and is regarded as a major water reservoir in the deep Earth [3]. The core-mantle boundary, which separates the solid mantle and the liquid outer core, is reported to have water in specific zones where H is further transported and infiltrated to the core through mineral chemistry reactions [4]. If water is transported from the hydrous transition zone to the core, the mid-layer, with a great portion belonging to the mid-lower mantle (660–1700 km), should leave clues of water transportation detected by global tomography data. For this purpose, the location of hydrous pocket, the abundance of water, and the mineralogy of water-bearing phases are constrained by their seismic [5] and/or electromagnetic [6] properties. The incorporation of hydrous phase may explain large-scale seismic structures in the deep lower mantle [7]. Hundreds of kilometers above, the mid-lower mantle is regarded as nominally seismically and electrically homogeneous [8], and only small-scale heterogeneity could exist [9–11]. Such heterogenous scatterers may be responsible for water transportation.

The electrical conductivity (EC) and seismic wave velocity profiles of Earth's lower mantle have been mapped out using global three-dimensional (3D) and one-dimensional (1D) induction and seismic studies [8,9,11,12], in which a couple of areas in the mid-lower mantle with abnormal EC and velocity values were located. The global 3D model showed high conductivity scatterers with up to 10^2 S/m at depths of 900–1400 km beneath eastern Africa, South-east Asia, and Eurasia, in stark contrast to some large low conductivity areas (10^{-2} S/m) under the Australian region, Western Africa, near Japan, north and central America [8,12]. At similar depths (800–1300 km), slow seismic velocity scatterers were

* Corresponding authors.
E-mail addresses: zhangyoujun@scu.edu.cn (Y. Zhang), qingyang.hu@hpstar.ac.cn (Q. Hu).
[1] These authors contributed equally to this work.

https://doi.org/10.1016/j.scib.2021.12.002
2095-9273/

found in Central America, the Indian subcontinent, and South Pacific [10]. The tomographic information is visualized in the referenced multi-dimensional maps of Fig. 1, showing the variations of seismic and EC on the global scale. The two maps of seismic velocity and EC were then overlayed in different color scales to highlight scatterers with both high conductivity and low-velocity properties (Fig. 1a). However, sourcing those double-constrained anomalies is technically challenging [14]. The ECs of major minerals including bridgmanite (Bgm) and ferropericlase (Fp) leave a notable gap with the high EC values in mid-lower mantle scatterers [15,16], even considering iron/aluminum-bearing effects [15]. With the further constraints from sound velocity properties (e.g., longitudinal (V_p) and shear (V_s) velocity), very few mineral phases are known to be responsible for those observations, which feature both low V_p and high EC [17].

Seismological anomalies in the mantle, such as pervasive scatterers throughout the mid-lower mantle (from 800 to 1300 km) [10], are often correlated with abnormal EC values. Therefore, coupled EC and sound velocity measurements from mineralogy experiments provide robust constraints on the mineralogy origins. Recent studies suggested that iron-enriched materials or dense hydrous phases may be responsible for such observations. For example, the subducted oceanic crust may contain a large amount of water [7] and contribute to the high electrical conductivity [6] and high-velocity heterogeneities in the mid-lower mantle [10]. The enrichment of ferric iron in the lower mantle is another critical factor. The iron end members such as Fe_2O_3 [18] and the superionic FeO_2H [19,20] are highly conductive at the relevant pressure–temperature (*P-T*) conditions of the bottom lower mantle. The seismic ($\delta \ln V_s/\delta \ln V_p$) of pyrite-type FeO_2H_x also exhibited excellent agreement with the ultra-low velocity zones at the margin of large low shear velocity provinces (LLSVPs) [5]. The polymorphic transition from ε-FeOOH to pyrite-type FeO_2H and the following dehydrogenation suggest a journey of transporting FeOOH throughout the entire mantle, which may generate heterogeneity along its way in the mid-lower mantle. In this work, we observed high EC and low V_p of ε-FeOOH in the mid-lower mantle conditions and the minor mineral ε-FeOOH may serve as one of the water-bearing phases to carry water down to the lowermost mantle.

2. Results

2.1. Electrical conductivity of ε-FeOOH under pressure

High-pressure EC experiments of ε-FeOOH were performed up to 61.2 GPa in a diamond anvil cell (DAC) (Fig. 2a, Table S1 online). Under high pressure and ambient temperature conditions, we used impedance spectroscopy to measure the resistance (*R*) and then calculated its EC (details in Methods). The errors of the measured resistances in the Nyquist plot fitting were less than 1% (Table S1 online). Our results show that the EC of ε-FeOOH is $6.26(62) \times 10^{-3}$ S/m at ambient conditions and monotonously increases to $4.7(5) \times 10^{-1}$ S/m by pressurizing to around 43 GPa at room temperature. At approximately 45 GPa, it suddenly jumped up and reached $1.24(12) \times 10^{3}$ S/m at 61.2 GPa (Fig. 2a). The trend of EC in compressed ε-FeOOH was reproduced in two additional runs of experiments (Fig. 2). Such high EC is comparable to metallic compounds, for example, FeO ($4.8(12) \times 10^{4}$ S/m at ~70 GPa and 1850(180) K) [21] and FeH_x (~4×10^{5} S/m at 25.5 GPa and 200 K) [22].

We also conducted parallel EC measurements for δ-AlOOH and γ-AlOOH to investigate the effect of Fe^{3+}. For δ-AlOOH, its EC is nearly invariantly correlated with pressure up to 51(2) GPa (Fig. 2a). The EC of γ-AlOOH climbed with increasing pressure. In contrast to ε-FeOOH, the abrupt increase of EC at above 40 GPa was absent in both aluminum end members (Fig. 2). Therefore, the soaring EC in ε-FeOOH is likely due to the Fe cation and possibly the electronic spin transition (e.g., between 40 and 60 GPa) or the previously reported second-order phase transition from $P2_1nm$ to *P*nnm (43 GPa) [23].

We then studied the temperature effect on the EC of ε-FeOOH under high pressure (Fig. 2b). At pressures below 35.5 GPa, the EC of ε-FeOOH and temperature is positively correlated at least to 1500 K, which is a typical feature of semiconductor [24] (Fig. 2b and Table S2 online). The results are also consistent with previous studies at lower pressures using a Kawai-type multi-anvil press [25]. At above 50 GPa, the correlation between the EC and temperature was reversed. By laser heating to 1800 K, the EC of ε-FeOOH decreased by approximately a factor of two compared with that at ambient temperature. This reduction of EC was robustly reproduced in three independent runs of laser-heating experiments and also agreed with an external heating experiment up to 500 K in a resistance-heated DAC (Fig. S1 online). This is clear evidence of a semiconductor–metal transition in ε-FeOOH [26].

The Nyquist plots also provide key information on the progress of the phase transition in ε-FeOOH (Fig. 3a, b). Semiconductor ε-FeOOH has one semi-circle in the high-frequency region (Fig. 3a). The type of conduction mechanism belongs to the small polaron hopping conduction, similar to other hydroxide or hydrous minerals [27]. At 53.5 GPa, a second semi-circular arc appeared in the low-frequency region next to the main circle (Fig. 3b). The onset of the second arc is attributed to grain boundary resistance [24] and was previously regarded as a symbol of the charge carrier transportation anisotropy in the crystallites [28]. While both *in situ* X-ray diffraction experiments and literature data indicate that ε-FeOOH is a stable phase throughout the pressures investigated by the present study [23,29] (Fig. S2 online), the second arc is most likely originated from the spin-pairing of Fe^{3+} [23], which may create a mixed spin-state.

2.2. The metallization of ε-FeOOH from theory

We then conducted comprehensive density function theory (DFT) and dynamic mean-field theories (DMFT) calculations to reveal the underlying electronic transition. Our computed band structure showed that the Fermi level crossed the valence band when the unit cell volume was below 51.27 $Å^3$ (or 50 GPa from DFT) where ε-FeOOH was in a low-spin configuration. The bandgap closure signifies clear evidence of metallization (Fig. 3c, d, and Fig. S3 online). The metallization is mainly associated with the redistribution of Fe d orbitals and shifting Fermi level to the valence bands due to the suppression of the Mott-Hubbard energy upon entering the low-spin state of Fe^{3+}, analogous to Fe_2O_3 [18] and $BiFeO_3$ [30]. Our results are consistent with a recent spectroscopic study on the bandgap energies of ε-FeOOH under pressure, which showed a pressure-induced bandgap reduction at spin transition pressures [26]. It is reported that thermal or large quantum fluctuations between the high and low-spin states can be enhanced by the presence of a wide 4s band right above the Fermi level, which may result in the outward expression of the conductive mechanism changing from small-polaron hopping to the free-electron conduction (the conduction mechanism of metal) in ε-FeOOH [21]. Similarly, our experiment confirmed the co-existence of two conduction mechanisms. During the spin transition, the arc at the low-frequency region became insignificant with increasing pressure (Fig. 3b), indicating that the free electron model started to dominate. Such waxing and waning also implies the progression of the spin transition and may further influence its seismic features.

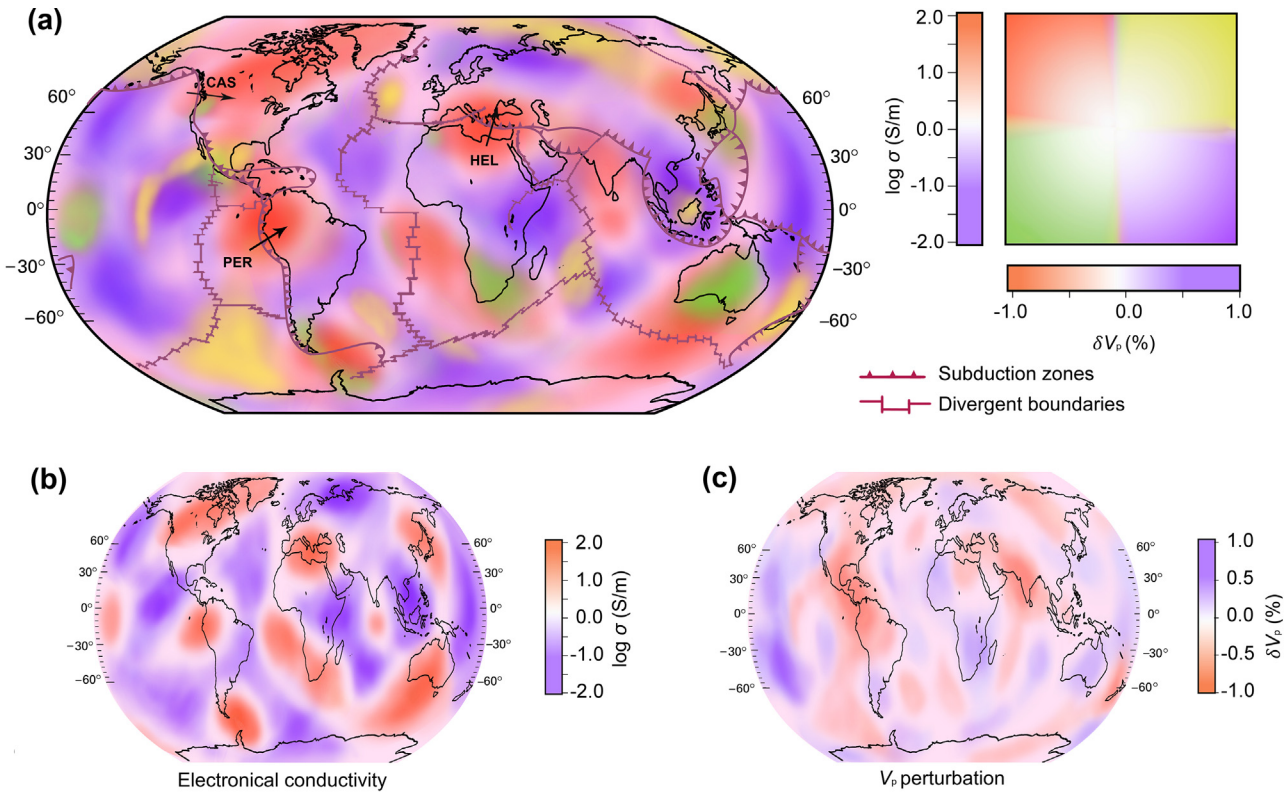

Fig. 1. Modeling of the heterogeneous electrical conductivity (EC) and P-wave seismic velocity at the layer of 1220 km in the mid-lower mantle. (a) Combined EC and V_p model. (b) The conductivity model is from Tarits and Mandéa [12]. (c) The P-wave model is from Becker and Boschi [11]. Red areas represent the high EC with low seismic velocity scatterers, blue areas represent the low EC with high-velocity scatterers, yellow areas represent the high EC with high-velocity scatterers, and green areas represent the low EC with low-velocity scatterers. Brown red lines are the schematic subduction zones and divergent boundaries [13]. The three black arrows are CAS: Cascadia slab, PER: Peru slab, and HEL: Hellenic slab.

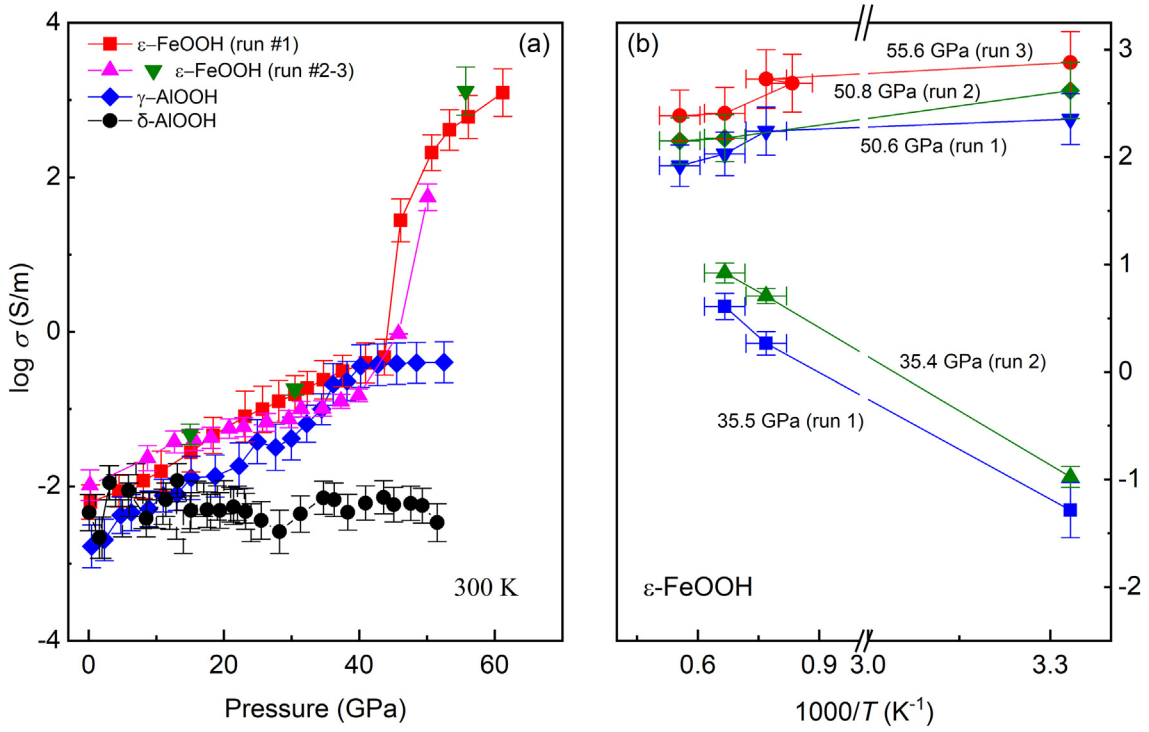

Fig. 2. Electrical conductivity of ε-FeOOH at high pressure–temperature. (a) Electrical properties of ε-FeOOH, γ-AlOOH, and δ-AlOOH versus pressure at 300 K. The EC of ε-FeOOH jumped higher at 50 GPa. The errors of EC are no more than 10%. Pressure uncertainty is ± 0.5 GPa. (b) The EC of ε-FeOOH as a function of temperature at high pressure.

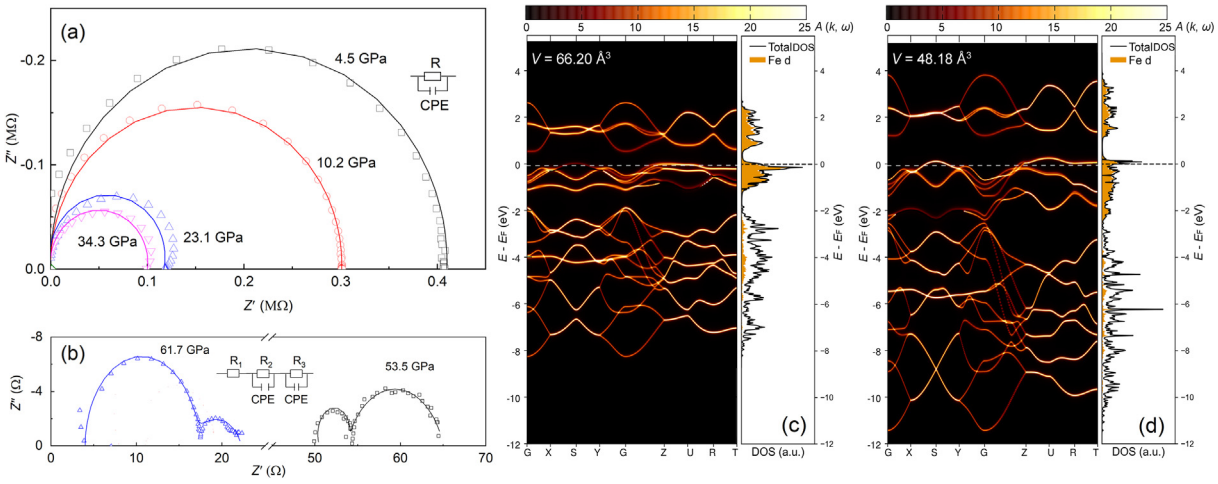

Fig. 3. Selected Nyquist plots of ε-FeOOH under compression and the calculated band structure and density of states at ambient and high pressure. (a) The equivalent circuit consists of a single part of one resistor and one constant phase element (R-CPE) in parallel below 50 GPa; (b) at 53.5 GPa, the equivalent circuit splits into three parts. The solid curves in (a) and (b) are the corresponding fitting curves with equivalent circuits shown in the corner or top of the figure. (c) Calculated band structure and density of states of ε-FeOOH at fixed volumes of 66.20 (c) and 48.18 Å^3 (d) with temperature at 300 K, where the lattice volume corresponds to ambient pressure and 50 GPa, respectively. The projected density of states is plotted in Fig. S3 (online). At ambient pressure, ε-FeOOH is a narrow gap (0.65 eV) semiconductor. At 50 GPa, ε-FeOOH is a correlated metal, and the onset of Fe d orbitals mainly contributed to the metallization of ε-FeOOH.

2.3. Sound velocity of ε-FeOOH across the spin-transition region

In addition to our EC measurements, we measured the V_p of ε-FeOOH at high *P-T* by hypervelocity impact using a 25-mm-bore two-stage light-gas gun at the Institute of Atomic and Molecular Physics, Sichuan University (see Methods online). The measured V_p increased with pressure up to 42.8(20) GPa (Fig. 4). With further increasing pressure, it dropped by 16.8% at pressures of 45–60 GPa (Fig. 4 and Table S3 online), where the spin transition of Fe^{3+} occurred [33]. Finally, the V_p could recover to a normal level at pressures beyond the spin transition [33]. The change of V_p was verified by our first-principles simulation based on the vibrational virtual crystal model (see Methods online), which qualitatively reproduced the softening of V_p upon the mixed spin states (Fig. 4). Compared to the Preliminary Reference Earth Model (PREM), the V_p of ε-FeOOH is up to 29.5% lower at 53(2) GPa and 1100(100) K which has been occasionally found in the mid-lower mantle [17]. Our results confirmed that the electronic transition of ε-FeOOH not only significantly increases its EC but may also exhibit strong anomalies in its sound velocities.

It is worth noting that the EC and sound velocity are two major variables that can be directly monitored from the surface as constraints to the physical properties of Earth's deep interiors. The EC of low-spin, metallic ε-FeOOH is nearly two orders of magnitudes higher than that of iron-bearing bridgmanite (Bgm) at 50 GPa and 1800 K (Fig. S4 online). Compared with other ferric systems, for instance, the $Mg_{0.83}Fe_{0.21}Al_{0.06}Si_{0.91}O_3$ [15] and $Mg_{0.60}Fe_{0.40}Si_{0.63}Al_{0.37}O_3$ Bgm [34], the increment of EC in FeOOH is much more substantial, owing to the Mott-type semiconductor to metal transition.

3. Discussion and conclusion

Spin transition theories in the mid-lower mantle were proposed almost two decades ago [35] and had profound implications for interpreting lower mantle heterogeneities. Previous studies show that the effects of spin transition on its physical properties are highly dependent on the iron content and the site of Fe in the lattice [18]. For example, the A-site of the perovskite-structured phases in iron-bearing Bgm is more pressure-reluctant to enter the low-spin state than the B-site, making its valence and spin states "invisible" [36]. Spin-paring of Fe^{2+} is also reported to lower the EC of Fp across the high-low spin transition regime as the low-spin state slows the mobility of the charge transfer carriers [16]. In our case of ε-FeOOH, the low-spin state exhibited a dramatic decrease in the Mott-Hubbard energy, which eventually led to an electronic transition from semiconductor to metal [18,30].

Similar to the spin transition of Fp and iron-bearing Bgm, our measured mixed spin-state induced a much more substantial drop in V_p than the seismic variations (up to 4%–5%) of the mid-lower mantle derived by seismology [17]. This is because the softening of the mixed spin-state on seismic velocities is attenuated at higher temperatures [37] (Table S3 online). The most prominent reduced V_p in the mid-lower mantle found in the Cascadia slab (CAS, the subducted depth may reach ~1500 km), Peru slab (PER, the depth is ~1500 km), and Hellenic slab (HEL, the depth is ~1000 km) [13] are reasonably explained by the occurrence of a mixed spin-state of iron. However, seismic data alone is not enough to further distinguish the mineral composition.

The electrical conductivity change provides a second layer of constraint in predicting the mineralogical origin of heterogenous scatterers in the mid-lower mantle. This is important as the multi-dimensional mapping of lower-mantle properties is fundamental to understanding the accretion, differentiation, and thermochemical evolution of our planet. Echoing the global tomographic data (Fig. 1a), regions colored in red with high EC and low V_p are found beneath the South-east Indian Ocean, India, Mediterranean, South Atlantic, Northern South America, and Northern North America at the mid-lower mantle [12]. The increase of EC with depth in those scatterers is much greater than other regions in the mid-lower mantle [38]. To our best knowledge, this fits the trend of EC in ε-FeOOH, and possibly its dehydrated Fe_2O_3 [18], both of which have shown metallization in the sensitive pressure regimes. While the electronic phase transition in Fe_2O_3 is site-selective and has a higher (>72 GPa) spin transition pressure [18], the reduction of V_p by the mixed spin-states is unlikely applying to Fe_2O_3.

The correlation of abnormal EC and V_p scatterers has an intriguing coincidence with the location of tectonic plates (Fig. 1a). Subduction slabs are dynamic sites of mass and energy exchange in between the Earth's surface and its interiors. The delivery of crustal materials to the mantle follows different types of subducted

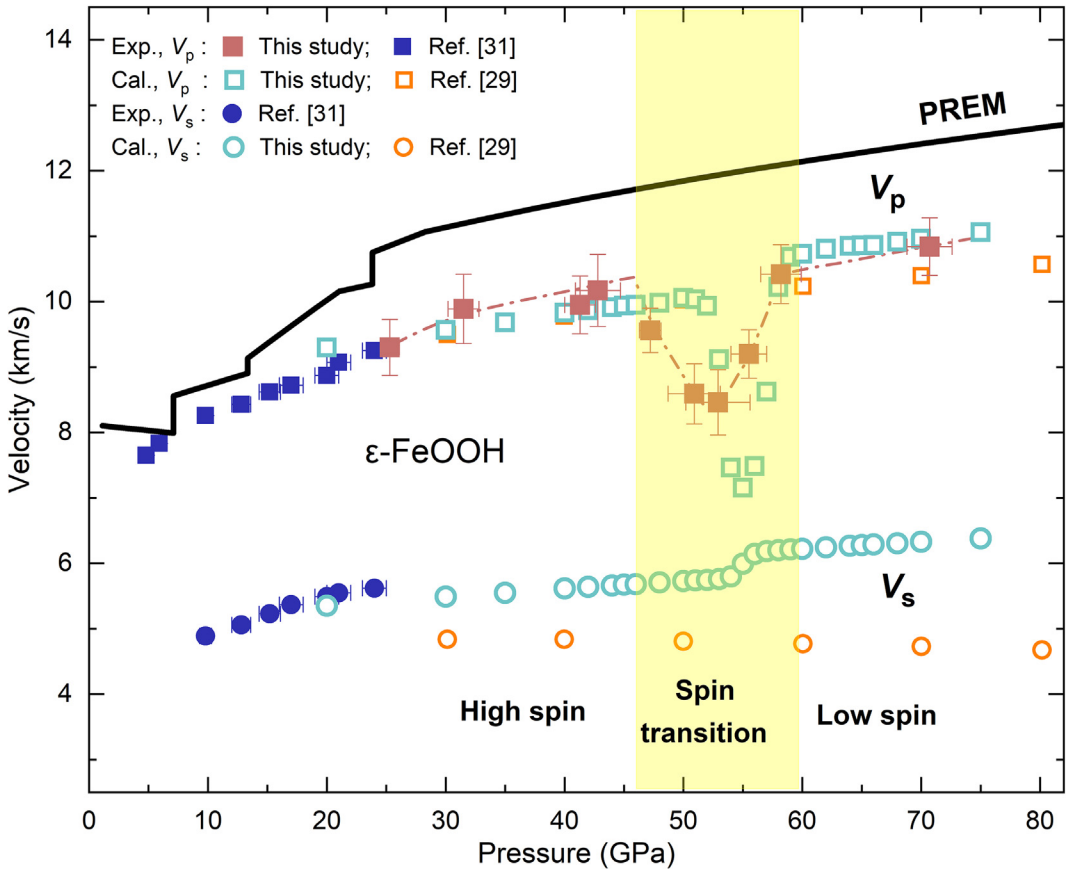

Fig. 4. Sound velocities of ε-FeOOH at high pressure–temperature conditions. The solid brown squares represent our determined V_p by shock compression experiments. The solid blue squares and circles represent V_p and V_s of ε-FeOOH at high pressure and room temperature by Ikeda et al. [31], respectively. The open orange squares and circles represent our calculated V_p and V_s at high pressure and 900 K, respectively. The open green squares and circles are V_p and V_s at high pressure calculated by Thompson et al. [29] using density functional theory with a Coulombic self-interaction term (U) at 0 K. The solid black line represents the V_p of seismic observations from PREM [32]. The brown dash-dotted line is a guide to the eye, showing the trend of our experimentally determined V_p. The light-yellow shaded area (46–60 GPa) stands for the spin transition zone with a mixed-spin state.

processes, such as metamorphism, metasomatism, and magmatism, which will cause heterogeneity in the chemical composition [39] and lead to velocity and EC anomalies. The low V_p anomaly is generally 4% slower in those slabs [11,40], which, from a mineralogy perspective, is possibly induced by the incorporation of some minor phases. Many other possibilities can also cause EC or seismic heterogeneity. For instance, hot mantle upwelling could result in sub-slab low-velocity anomalies [40]. However, the evolution of EC will help us to further refine the available sources. We noticed that many high EC, low V_p scatterers described above are located at the slab beneath subduction zones such as CAS, PER, and HEL that extend to the mid-lower mantle [13]. High-pressure mineral physics experiments by McCammon et al. [41] also support that the concentration of Fe^{3+} and water content is positively correlated, such that those scatterers are likely to be enriched in water and ferric iron. On the basis of our analysis, the concentration of ε-FeOOH may be much higher than previously thoughts in such scatterers. If we assume a scenario of mixing ε-FeOOH to a mid-oceanic ridge basalt (MORB) composition at the bottom of subduction slabs, 5%–10% of ε-FeOOH to a MORB composition yields a total EC of 11.2 ± 1.6 to 12.5 ± 1.8 S/m at 51 GPa by using the simple averaging theorem [42]. Meanwhile, the 5%–10% mixture can also lower the velocity of MORB to explain the V_p perturbation (Fig. 1c) in the mid-lower mantle [43]. At a deeper depth beyond the stability of ε-FeOOH, it will decompose and/or carry over water to other dense hydrous phases [44–46]. The local enrichment of ε-FeOOH in the mid-lower mantle may be responsible for connecting the water in the mantle transition zone and the core-mantle boundary. Therefore, the accurate location and abundance of ε-FeOOH in the deep mantle have important implications for the water cycling throughout mantle.

To sum up, high pressure alters the spin state and electron conduction mechanism from semiconductor to metal in ε-FeOOH. Double constraints from high EC and low V_p make it a compelling candidate to explain featured heterogenous scatterers in the mid-lower mantle. Future studies of petrology and deep diamond inclusions are in demand to detect and put further constraints on the availability of iron-enriched hydrous materials in the mid-lower mantle.

Conflict of interest

The authors declare that they have no conflict of interest.

Acknowledgments

We acknowledge that Yingwei Fei (Carnegie Institution of Washington) facilitated the project and provided support for sample synthesis. We thank Ms. Freyja O'Toole (Center for High Pressure Science and Technology Advanced Research, HPSTAR) for language editing, Kuo Li (HPSTAR) for his support in conducting impedance measurements, Qiming Wang, Feng Gao, Xilong Dou, and Yuanyuan Li (Sichuan University) for their help in shock experiments, and Chunyin Zhou (Shanghai Advanced Research Institute,

Chinese Academy of Sciences) for our pilot synchrotron-based high-pressure experiments at the BL15U1 of Shanghai Synchrotron Radiation Facility. Yukai Zhuang is supported by the Research Start-up Funds of Talents of Sichuan University (1082204112667) and China Postdoctoral Science Foundation (18NZ021-0213-216308). Catalin Popescu is supported by Spanish Mineco Project (FIS2017-83295-P). Mingqiang Hou is supported by the Strategic Priority Research Program of Chinese Academy of Sciences (XDB41000000). Qingyang Hu is supported by the China Academy of Engineering Physics Research Project (CX20210048) and a Tencent Xplorer Prize. Youjun Zhang is partially supported by the National Natural Science Foundation of China (42074098) and the United Laboratory of High-pressure Physics and Earthquake Science (HPPES202001). HPSTAR operations are partially supported by the National Natural Science Foundation and the China Academy of Engineering Physics Joint Fund (U1530402).

Author contributions

Yukai Zhuang, Bo Gan, Zhongxun Cui, Ruilian Tang, Catalin Popescu, Gaston Garbarino, Youjun Zhang, and Qingyang Hu conducted the high pressure–temperature experiments. Qingyang Hu performed the theoretical simulation. Renbiao Tao synthesized the sample. Mingqiang Hou and Gang Jiang provided experimental protocols. Yukai Zhuang, Youjun Zhang, and Qingyang Hu wrote the paper with input from all co-authors. Qingyang Hu and Youjun Zhang conceived the work.

Appendix A. Supplementary materials

Supplementary materials to this article can be found online at https://doi.org/10.1016/j.scib.2021.12.002.

References

[1] Ohtani E. Water in the mantle. Elements 2005;1:25–30.
[2] Hu Q, Liu J, Chen J, et al. Mineralogy of the deep lower mantle in the presence of H_2O. Natl Sci Rev 2021;8:nwaa098.
[3] Bercovici D, Karato S-I. Whole-mantle convection and the transition-zone water filter. Nature 2003;425:39–44.
[4] Nishi M, Kuwayama Y, Tsuchiya J, et al. The pyrite-type high-pressure form of FeOOH. Nature 2017;547:205–8.
[5] Liu J, Hu Q, Kim DY, et al. Hydrogen-bearing iron peroxide and the origin of ultralow-velocity zones. Nature 2017;551:494–7.
[6] Ohta K, Hirose K, Ichiki M, et al. Electrical conductivities of pyrolitic mantle and MORB materials up to the lowermost mantle conditions. Earth Planet Sci Lett 2010;289:497–502.
[7] Lin Y, Hu Q, Meng Y, et al. Evidence for the stability of ultrahydrous stishovite in Earth's lower mantle. Proc Natl Acad Sci USA 2020;117:184–9.
[8] Kuvshinov A, Olsen N. A global model of mantle conductivity derived from 5 years of CHAMP, Ørsted, and SAC-C magnetic data. Geophys Res Lett 2006;33:L18301.
[9] Constable S, Constable C. Observing geomagnetic induction in magnetic satellite measurements and associated implications for mantle conductivity. Geochem Geophys Geosyst 2004;5:Q01006.
[10] Waszek L, Schmerr NC, Ballmer MD. Global observations of reflectors in the mid-mantle with implications for mantle structure and dynamics. Nat Commun 2018;9:385.
[11] Becker TW, Boschi L. A comparison of tomographic and geodynamic mantle models. Geochem Geophys Geosyst 2002;3:2001GC000168.
[12] Tarits P, Mandéa M. The heterogeneous electrical conductivity structure of the lower mantle. Phys Earth Planet Inter 2010;183:115–25.
[13] Goes S, Agrusta R, van Hunen J, et al. Subduction-transition zone interaction: a review. Geosphere 2017;13:644–64.
[14] Zhang B-H, Guo X, Yoshino T, et al. Electrical conductivity of melts: implications for conductivity anomalies in the Earth's mantle. Natl Sci Rev 2021:nwab064.
[15] Sinmyo R, Pesce G, Greenberg E, et al. Lower mantle electrical conductivity based on measurements of Al, Fe-bearing perovskite under lower mantle conditions. Earth Planet Sci Lett 2014;393:165–72.
[16] Lin J-F, Weir ST, Jackson DD, et al. Electrical conductivity of the lower-mantle ferropericlase across the electronic spin transition. Geophys Res Lett 2007;34:L16305.
[17] Kaneshima S, Helffrich G. Dipping low-velocity layer in the mid-lower mantle: evidence for geochemical heterogeneity. Science 1999;283:1888–92.
[18] Greenberg E, Leonov I, Layek S, et al. Pressure-induced site-selective mott insulator-metal transition in Fe_2O_3. Phys Rev X 2018;8:031059.
[19] Hou M, He Y, Jang BG, et al. Superionic iron oxide-hydroxide in Earth's deep mantle. Nat Geosci 2021;14:174–8.
[20] Hu Q, Mao H-K. Role of hydrogen and proton transportation in Earth's deep mantle. Matter Radiat Extremes 2021;6:068101.
[21] Ohta K, Cohen RE, Hirose K, et al. Experimental and theoretical evidence for pressure-induced metallization in FeO with rocksalt-type structure. Phys Rev Lett 2012;108:026403.
[22] Matsuoka T, Hirao N, Ohishi Y, et al. Structural and electrical transport properties of FeH_x under high pressures and low temperatures. High Press Res 2011;31:64–7.
[23] Gleason AE, Quiroga CE, Suzuki A, et al. Symmetrization driven spin transition in ε-FeOOH at high pressure. Earth Planet Sci Lett 2013;379:49–55.
[24] Zhuang Y, Dai L, Wu L, et al. Pressure-induced permanent metallization with reversible structural transition in molybdenum disulfide. Appl Phys Lett 2017;110:122103.
[25] Wang R, Yoshino T. Electrical conductivity of diaspore, δ-AlOOH and ε-FeOOH. Am Miner 2021;106:774–81.
[26] Thompson EC, Davis AH, Brauser NM, et al. Phase transitions in ε-FeOOH at high pressure and ambient temperature. Am Miner 2020;105:1769–77.
[27] Kaneko K, Inoue N, Ishikawa T. Electrical and photoadsorptive properties of valence-controlled α-iron hydroxide oxide. J Phys Chem 1989;93:1988–92.
[28] Wang L, Ke F, Wang Q, et al. Effect of crystallization water on the structural and electrical properties of $CuWO_4$ under high pressure. Appl Phys Lett 2015;107:201603.
[29] Thompson EC, Campbell AJ, Tsuchiya J. Elasticity of ε-FeOOH: seismic implications for Earth's lower mantle. J Geophys Res Solid Earth 2017;122:5038–47.
[30] Gavriliuk AG, Struzhkin VV, Lyubutin IS, et al. Another mechanism for the insulator-metal transition observed in mott insulators. Phys Rev B 2008;77:155112.
[31] Ikeda O, Sakamaki T, Ohashi T, et al. Sound velocity measurements of ε-FeOOH up to 24 GPa. J Mineral Petrol Sci 2019;114:155–60.
[32] Dziewonski AM, Anderson DL. Preliminary reference Earth model. Phys Earth Planet Inter 1981;25:297–356.
[33] Wu Z, Justo JF, Wentzcovitch RM. Elastic anomalies in a spin-crossover system: ferropericlase at lower mantle conditions. Phys Rev Lett 2013;110:228501.
[34] Potapkin V, McCammon C, Glazyrin K, et al. Effect of iron oxidation state on the electrical conductivity of the Earth's lower mantle. Nat Commun 2013;4:1427.
[35] Badro J, Fiquet G, Guyot F, et al. Iron partitioning in Earth's mantle: toward a deep lower mantle discontinuity. Science 2003;300:789–91.
[36] Liu J, Dorfman SM, Zhu F, et al. Valence and spin states of iron are invisible in Earth's lower mantle. Nat Commun 2018;9:1284.
[37] Shukla G, Wentzcovitch RM. Spin crossover in $(Mg, Fe^{3+})(Si, Fe^{3+})O_3$ bridgmanite: effects of disorder, iron concentration, and temperature. Phys Earth Planet Inter 2016;260:53–61.
[38] Civet F, Thébault E, Verhoeven O, et al. Electrical conductivity of the Earth's mantle from the first swarm magnetic field measurements. Geophys Res Lett 2015;42:3338–46.
[39] Zheng Y-F. Subduction zone geochemistry. Geosci Front 2019;10:1223–54.
[40] Fan J, Zhao D. Subslab heterogeneity and giant megathrust earthquakes. Nat Geosci 2021;14:349–53.
[41] McCammon CA, Frost DJ, Smyth JR, et al. Oxidation state of iron in hydrous mantle phases: implications for subduction and mantle oxygen fugacity. Phys Earth Planet Inter 2004;143-144:157–69.
[42] Deschamps F, Khan A. Electrical conductivity as a constraint on lower mantle thermo-chemical structure. Earth Planet Sci Lett 2016;450:108–19.
[43] Zhao M, Zhou H, Yin K, et al. Thermoelastic properties of aluminous phases in MORB from first-principles calculation: implications for Earth's lower mantle. J Geophys Res Solid Earth 2018:10583–96.
[44] Zhu SC, Hu Q, Mao WL, et al. Hydrogen-bond symmetrization breakdown and dehydrogenation mechanism of FeO_2H at high pressure. J Am Chem Soc 2017;139:12129–32.
[45] Gan B, Zhang Y, Huang Y, et al. Partial deoxygenation and dehydration of ferric oxyhydroxide in Earth's subducting slabs. Geophys Res Lett 2021;48:e2021GL094446.
[46] Koemets E, Fedotenko T, Khandarkhaeva S, et al. Chemical stability of FeOOH at high pressure and temperature, and oxygen recycling in early Earth history. Eur J Inorg Chem 2021;2021:3048–53.

Yukai Zhuang received his Ph.D. degree at Institute of Geochemistry, Chinese Academy of Sciences in 2018. After completing the post-doctoral work in Center for High Pressure Science and Technology Advanced Research in 2020, now he is working at Sichuan University as an associate professor. His research interest mainly focuses on the structural, electronic and geological properties of minerals and rocks under high pressure.

Bo Gan is a Ph.D. candidate at Institute of Atomic and Molecular Physics, Sichuan University. He mainly works on the physical properties of hydrous minerals, iron oxides, and iron alloys under high temperatures and high pressures using dynamic shock compression experiments.

Youjun Zhang graduated from Northwestern Polytechnical University in 2009 and obtained his Ph.D. degree at Hiroshima University in 2015. He is an associate professor at Sichuan University and Chengdu University of Technology. He mainly focuses on studying the physical property of geological material and condensed matter under extreme conditions by static and dynamic compression to reveal the geophysics and geodynamics of Earth's interior and planetary bodies.

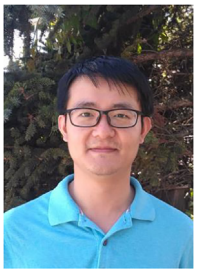

Qingyang Hu obtained Ph.D. degree from George Mason University in 2014 and is currently a staff scientist at Center for High Pressure Science and Technology Advanced Research. He conducts experiment and simulation to study mineral properties and their large-scale impacts at the conditions of Earth's deep interiors. Specifically, he is interested in the water-bearing systems of dense hydrous phases and silica, which will help to increase margins of deep Earth geophysics, geochemistry, and geodynamics.